

# Innovative Numerical Methods for Nonlinear MEMS: the Non-Incremental FEM vs. the Discrete Geometric Approach

P. Bettini, E. Brusa, M. Munteanu, R. Specogna and F. Trevisan<sup>1</sup>

**Abstract:** Electrostatic microactuator is a paradigm of MEMS. Cantilever and double clamped microbeams are often used in microswitches, microresonators and varactors. An efficient numerical prediction of their mechanical behaviour is affected by the nonlinearity of the electromechanical coupling. Sometimes an additional nonlinearity is due to the large displacement or to the axial-flexural coupling exhibited in bending. To overcome the computational limits of the available numerical methods two new formulations are here proposed and compared. Modifying the classical beam element in the Finite Element Method to allow the implementation of a *Non incremental sequential approach* is firstly proposed. The so-called *Discrete Geometric Approach (DGA)*, already successfully used in the numerical analysis of electromagnetic problems, is then applied. These two methods are here formulated, for the first time, in the case of strongly nonlinear electromechanical coupling. Numerical investigations are performed to find the pull-in of microbeam actuators experimentally tested. The non incremental approach is implemented by discretizing both the structure and the dielectric region by means of the FEM, then by meshing the electric domain by the Boundary Element Method (BEM). A preliminary experimental validation is finally presented in the case of planar microcantilever actuators.

**Keyword:** MEMS, Electromechanical coupled problem, FEM, BEM, DGA

## 1 Introduction

A key feature of microsystem design is the efficient use of electromechanical coupling for actuation, sensing and energy harvesting purposes [Senturia (2001); Rebeiz (2003)]. Scale laws demonstrate that the strongest actions can be reached by applying the electric field to flexible microstructures [De Bona and Enikov (2006)].

---

<sup>1</sup> Dept. Electrical, Management and Mechanical Eng. (DIEGM) and Lab. Ubiquita and Pervasive Technologies (Tech-Up), Università di Udine, Udine, Italy

Cantilever and double clamped microbeam actuators are therefore widely used in MEMS. They are deflected by the electric field in microswitches, microresonators and variable capacitors (varactors). Unfortunately, these devices suffer the breakdown and pull-in phenomena, which lead to the collapse of the structure [Senturia (2001); Rebeiz (2003)]. Their prediction is never simple, since electrostatic force exhibits an intrinsic nonlinearity, which depends on voltage, charge and mechanical displacement. The equilibrium equations couple electrical and mechanical degrees of freedom, in static and dynamic domains. This problem is nonlinear and often requires a numerical solution. The literature developed analytical and numerical approaches [Senturia (2001); Rebeiz (2003)]. Numerical solutions are mainly based on the Finite Element Method (FEM) and Boundary Element Method (BEM). In practice, the analytical approaches are effective only in case of very simple geometries, while the numerical methods need for iterative solutions in the presence of nonlinearity [Gyimesi and Ostergaard (1999)]. Quite often a deep mesh refinement and morphing operations are required [Adey, Lahrman, and Le mölmann (1995)]. Moreover, a so-called *geometrical* nonlinearity of the structure is sometimes present. This effect is well known in mechanical structures. Usually it appears in case of large displacements and deformations. This was already dealt with by Sen Yun Lee [Lee, Lin, Lee, Lu, and Liu (2008)] in case of analytical modelling of beams, by using shifting functions to increase the performance of the solution, and by Wen [Wen and Hon (2007)] in case of geometrical nonlinearity of plates, by using meshless approaches. In presence of electromechanical coupling these methods look unsuitable to include the nonlinearity of the electromechanical action, superimposed to the mechanical nonlinearity. In particular, analytical methods demonstrated to be ineffective to predict the pull-in phenomenon of these geometrically nonlinear microsystems. More interesting appears the BEM formulation described in [Springhetti, Novati, and Margonari (2006)], at least from the point of view of the numerical approach, although it applies in that case to plates and shells. Nevertheless, a complete formulation for nonlinear coupled problems is still to be developed. In microbeam actuators geometrical nonlinearity is caused either by the large displacement in bending, in case of microcantilever, or by the beam stretching in flexural behaviour, in case of double clamped configuration [Abdel-Raman, Younis, and Nayfeh (2003)]. The mechanical stiffness in both these cases changes and depends on the deformed shape of the structure [Munteanu, De Bona, Collenz, and Brusa (2004); Somà, Collenz, De Bona, and Gugliotta (2004)]. Several computational strategies were proposed. A full coupled FEM modelling including both the microstructure and the dielectric material is applied and the solution is found iteratively by means of Newton Raphson's technique. At each step the Jacobian matrix is computed and the problem is locally linearized [Adey, Lahrman, and Le mölmann (1995); De Bona and Enikov (2006)]. Computational time in

this case is large, particularly if 3D models are implemented. A so-called *sequential* solution is proposed to decrease the computational time [De Bona and Enikov (2006)]. An iterative procedure solves separately the electric and the mechanical problems, discretized either both by FEM or by FEM (mechanical) and BEM (electrical). For a given deformed shape of the structure the electric potential and the electromechanical forces are computed and imposed to the microsystem. The mechanical problem is then solved, displacements and rotations are computed. The two separated solutions are faster, but the number of iterations to predict the actual equilibrium condition may be large. Some improvements were investigated in [Somà, Collenz, De Bona, and Gugliotta (2004)]. Voltage and force increments were compared. A so-called *direct* solution was proposed in [Gyimesi and Ostergaard (1999)] and implemented in the ANSYS code. Electromechanical forces are computed first, for each foreseen deformed shape of the microsystem, and stored. The code simply inputs the computed forces in the nonlinear mechanical solution process. This strategy appears approximated, when pull-in voltage and displacement are computed. Only the structure is discretized by finite elements, while the dielectric region is described by lumped parameter models. In fact, the sequential approach, with FEM and BEM meshing and voltage increments, looks the most effective in 2D modelling [Somà, Collenz, De Bona, and Gugliotta (2004); De Bona and Enikov (2006)]. Nevertheless, the computational time is high, when all the above mentioned nonlinearities are active. The goal of this paper is investigating innovative approaches to predict accurately the behaviour of microbeam actuators, by simplifying the computational procedure and increasing the performance.

## **2 The proposed approaches**

Two methodologies are herewith investigated to improve the efficiency of the sequential approach, in the applications where both the electromechanical and geometrical nonlinearities are present. A first one utilizes a special beam finite element [Barraco and Munteanu (2002a,b)], which allows to implement a *non incremental sequential* solution, even in presence of geometrical nonlinearity. This element does not apply a smoothing technique like in [Cui, Liu, Li, Zhao, Nguyen, and Sun (2008)], but selects a special set of nodal coordinates, instead of the classical displacements. In general, the prediction of the flexural behaviour of a microbeam is usually based on a second order differential problem, which assumes a linear differential relation between strain and displacement [Timoshenko (1968)]. This assumption fails when a geometrical nonlinearity occurs. In this case an iterative solution is implemented to predict the effects of the mechanical nonlinearity, while the sequential approach allows dealing with the nonlinear electromechanical coupling. In practice, a loop is required to find the instantaneous equilibrium

for each given distribution of the electromechanical force, when the sequential approach performs the corresponding step of the mechanical solution. The *non incremental* approach simplifies this operation by introducing a formulation of the theory of the beam which allows to avoid the implementation of the iterative part of the algorithm, even in presence of geometrically nonlinear structure. In practice, a special beam element is introduced whose nodal degrees of freedom (DoFs) include elongation and section rotation, instead of the flexural displacement. This formulation makes linear the problem, from the point of view of the geometrical nonlinearity [Barraco and Munteanu (2002a,b)]. It looks particularly effective in case of dynamic analysis, where an integration of the equations of motion over time is required. This can be implemented by means of the Newmark modified method, which interacts only with the sequential procedure tested in the static solution herewith described [Munteanu and Brusa (2005)]. A second approach is based on the possibility to simplify the discretization technique by means of a new formulation, which allows describing the coupled problem by means of algebraic equations instead of differential ones. This is referred to as Discrete Geometric Approach (DGA) [Tonti (1975); Bossavit (1998); Tonti (2001)]. It is tested in the case of planar electrostatic microactuators, by implementing the sequential algorithm. The DGA method was successfully applied in electrostatics [Bettini and Trevisan (2003)] and in plane elasticity problems [Cosmi (2001)] as well. Recently, a direct comparison between DGA and FEM in electrostatics has been presented in [Heshmatzadeh and Bridges (2007)]. The good results obtained candidate DGA to be applied to MEMS design [Bettini, Brusa, Munteanu, Specogna, and Trevisan (2008)]. Both the proposed approaches are validated by comparing the numerical results to those obtained by the FEM classic formulation and to some experimental evidences.

### **3 The non-incremental FEM approach**

The microcantilever actuator shall be used as paradigm to describe the non incremental strategy. It is a microbeam with length  $l$  and thickness  $t$ , which is electrostatically deflected by the voltage,  $V_0$ , applied between the structure itself and the ground electrode, through the gap,  $g$ . In case of dynamic behaviour voltage is variable over time. The problem is three dimensional, but is assumed to be plane. No fringing effect of the electric field is considered, at least at this level, along the width, which is assumed to be unitary. An half-plane domain is assumed to solve the electrostatic problem. In presence of suitable bending moment and gap, the tip displacement may be sufficiently large that the assumption of small displacement of the classic theory of the beam [Timoshenko (1968)] becomes inapplicable. In practice, the beam achieves a final equilibrium configuration so far from the initial

layout (Fig.1) that usually an incremental integration of the equilibrium equation is required. In this case the local gap of the transversal section A-A depends on the corresponding mechanical displacement. Loads are non-conservative, since the electric force distribution acts perpendicularly to the surface of the conductive beam. Therefore it changes direction and amplitude, depending on the deformed shape of the structure. Electromechanical forces are nonlinearly dependent on both the applied voltage and the gap distribution along the length of the deflected microbeam.

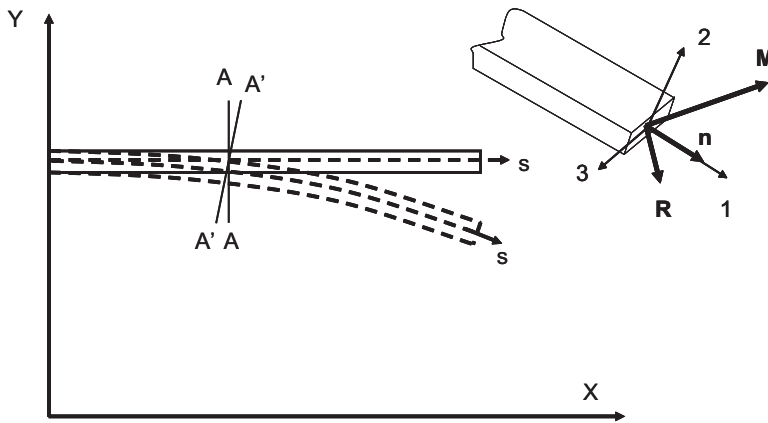


Figure 1: Description of the geometrically nonlinear behaviour of a cantilever microbeam electrostatically actuated. Reference frames for the FEM model are also shown.

### 3.1 Formulation of the non-incremental FE analysis

To analyse the deformed shape of a microbeam in presence of geometrical nonlinearity a curved configuration has to be considered. The set of differential equations describing the static equilibrium of a curved beam can be written according to [Baraco and Munteanu (2002a); Timoshenko (1968)] as:

$$\begin{aligned} \frac{d\mathbf{R}}{ds} + \mathbf{p} &= 0 \\ \frac{d\mathbf{M}}{ds} + \mathbf{n} \times \mathbf{R} + \mathbf{m} &= 0. \end{aligned} \tag{1}$$

Equations (1) are written in the local reference frame and  $s$  is the curvilinear coordinate of the beam centreline (Fig.1). Unit vector **n** is orthogonal to the selected

cross-section of the beam, referred to as A-A. Capital letters identify the resultant force  $\mathbf{R}$  and bending moment  $\mathbf{M}$ , acting on the beam cross-section. Vectors  $\mathbf{p}$  and  $\mathbf{m}$  correspond to the distributed forces and moments, acting along the axes of the microbeam. The expressions of all the above mentioned vectors are:

$$\mathbf{R} = \begin{bmatrix} N \\ T_2 \\ T_3 \end{bmatrix} \quad \mathbf{M} = \begin{bmatrix} M_t \\ M_2 \\ M_3 \end{bmatrix}, \tag{2}$$

$$\mathbf{p} = \begin{bmatrix} p_1 \\ p_2 \\ p_3 \end{bmatrix} \quad \mathbf{m} = \begin{bmatrix} m_1 \\ m_2 \\ m_3 \end{bmatrix}. \tag{3}$$

Subscripts 1, 2, 3 identify the local reference frame. In particular, axis referred to as 1 is orthogonal to the cross section A-A, while axes 2 and 3 are the central principal axes of the cross section.  $N$  is the axial effort applied along axis 1, while  $T_2$  and  $T_3$  are the shear actions along axes 2 and 3, respectively.  $M_t$  is the torsional moment about axis 1, while  $M_2$  and  $M_3$  are the two bending moments, about 2 and 3 respectively.

If the Timoshenko’s beam model is used to describe the mechanical behaviour of this system [Timoshenko (1968)], the cohesion forces  $\mathbf{R}$  and  $\mathbf{M}$  are linked to the strains by the Hooke’s laws, written in the local reference frame of the cross section:

$$\mathbf{R} = \mathbf{D}_0 \boldsymbol{\varepsilon} \quad \mathbf{M} = \mathbf{D} (\boldsymbol{\chi} - \boldsymbol{\chi}_0) = \mathbf{D} \Delta \boldsymbol{\chi}. \tag{4}$$

Bold letters are used to identify matrices and vectors, which include all the components of the strain and the curvatures. In particular,  $\boldsymbol{\chi}_0$  is the initial curvature of the undeformed shape of the beam. Strain and curvature vectors are:

$$\boldsymbol{\varepsilon} = \begin{bmatrix} \varepsilon_0 \\ \vartheta_2 \\ \vartheta_3 \end{bmatrix} \quad \boldsymbol{\chi} = \begin{bmatrix} \chi_t \\ \chi_2 \\ \chi_3 \end{bmatrix}, \tag{5}$$

where  $\varepsilon_0$  is the axial deformation, measured at the beam centreline, while  $\vartheta_2$  and  $\vartheta_3$  are the small shear angles between the plane orthogonal to the centreline and the two principal axes of the cross-section. Curvatures  $\chi_t$ ,  $\chi_2$  and  $\chi_3$  are related to the torsional and the two flexural curvatures, respectively. They describe the relative rotation in bending between two cross sections, being at an infinitesimal distance  $ds$ . Matrices  $\mathbf{D}_0$  and  $\mathbf{D}$  are respectively:

$$\mathbf{D}_0 = \begin{bmatrix} EA & 0 & 0 \\ 0 & GA_2 & 0 \\ 0 & 0 & GA_3 \end{bmatrix}, \quad (6)$$

$$\mathbf{D} = \begin{bmatrix} GI_t & 0 & 0 \\ 0 & EI_2 & 0 \\ 0 & 0 & EI_3 \end{bmatrix}. \quad (7)$$

$A_2$  and  $A_3$  are the effective areas used to evaluate shear effects on the cross section, while  $I_t$ ,  $I_2$  and  $I_3$  are the second order geometrical moments about the corresponding axes of the cross section.  $G$  and  $E$  are the transversal (tangential) and longitudinal (Young) elastic moduli.

If Eq.(4) is replaced in Eq.(1):

$$\begin{cases} \frac{d(\mathbf{D}_0\boldsymbol{\varepsilon})}{ds} + \boldsymbol{\chi} \times (\mathbf{D}_0\boldsymbol{\varepsilon}) + \mathbf{p} = 0 \\ \frac{d(\mathbf{D}\Delta\boldsymbol{\chi})}{ds} + \boldsymbol{\chi} \times (\mathbf{D}\Delta\boldsymbol{\chi}) + \mathbf{n} \times (\mathbf{D}_0\boldsymbol{\varepsilon}) + \mathbf{m} = 0. \end{cases} \quad (8)$$

This set of six equations allows finding the six unknown generalized displacements, i.e. three translations and three rotations.

In case of a two dimensional problem, as it is studied in present analysis, Eq.(8) becomes simpler:

$$\begin{cases} \frac{d(\mathbf{D}_0\boldsymbol{\varepsilon})}{ds} + \begin{bmatrix} -GA_2\vartheta_2\chi_3 \\ EA\varepsilon_0\chi_3 \end{bmatrix} + \mathbf{p} = 0 \\ \frac{d}{ds} \left[ EI_3 \left( \frac{d\theta}{ds} - \frac{d\theta_0}{ds} \right) \right] + GA_2\vartheta_2 + m_3 = 0. \end{cases} \quad (9)$$

Only three equations are included. There are two translational equilibrium conditions and one moment equilibrium equation. The actual curvature  $\chi_3$  and the curvature increment  $\Delta\chi$  can be expressed as function of the rotation angle  $\theta$  of the cross-section as:

$$\chi_3 = \frac{d\theta}{ds} \quad \Delta\chi = \frac{d\theta}{ds} - \frac{d\theta_0}{ds}, \quad (10)$$

where  $\theta_0$  is the slope of the undeformed shape of the beam.

The difference between the rotations referred to as  $\vartheta$  and  $\theta$ , respectively, can be appreciated in Fig.2. Vertical direction in Fig.2 is assumed to correspond to the undeformed shape of the microbeam. The actual rotation of the beam cross section corresponds to  $\theta$ . The latter can be interpreted as superposition of a pure rotation  $\varphi$ , imposed by the bending moment, and of the opposite rotation  $\vartheta$ , which is applied by the shear force, referred to as  $T$  [Timoshenko (1968)]. When the deformed shape of the beam is considered, an initial rotation  $\theta_0$  is already present and included in (10) to compute the actual values of curvature.

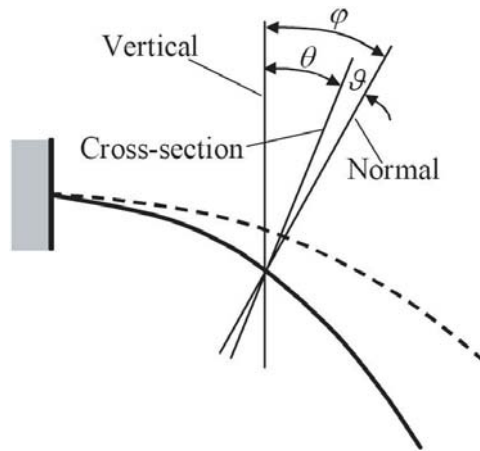


Figure 2: Description of the relevant angles in the beam model according to Timoshenko.

Nonlinear equations (8) and (9) are written for the deformed beam configuration. They are still valid even for large displacements. This allows an easier solution of the problem, because the incremental procedure is no more required to deal with the geometrical nonlinearity.

To find the expression of all the relevant matrices to be implemented into the FEM, the Virtual Work theorem is used [Timoshenko (1968)]:

$$\begin{aligned}
 \delta\Pi &= EA \int_1 \delta\varepsilon_0 \varepsilon_0 ds + GA_2 \int_1 \delta\vartheta \vartheta ds + \\
 &EI_3 \int_1 \delta\Delta\chi_3 \Delta\chi_3 ds - \int_1 \delta\mathbf{u}^T \mathbf{p} ds + \\
 &- \int_1 \delta\theta m_3 ds \\
 &= 0.
 \end{aligned}
 \tag{11}$$

The total potential energy of the system  $\delta\Pi$  is obtained as sum of all the contributions. They include the effects of the axial effort, of the shear and of the bending

moment, for a given length of the beam  $l$ . A term comes from the distributed force  $\mathbf{p}$ , being  $\mathbf{u}$  the displacement vector of the current point along the beam centreline. If the beam compliance is large, the contributions of  $N$  and  $T_2$  may be neglected. This assumption leads to the so-called Bernoulli beam model and equation (11) can be written as:

$$\delta\Pi = EI_3 \int_l \delta\Delta\chi_3\Delta\chi_3 ds + \int_l \delta\mathbf{u}^T \mathbf{p} ds - \int_l \delta\theta m_3 ds = 0. \tag{12}$$

The finite element used to predict the static behaviour of the system has only one degree of freedom per node, i.e. rotation  $\theta$ . All external loads, forces and moments, concentrated or distributed along the beam, are replaced by the equivalent nodal moments. According the theory of variations, Eq.(12) of the rotational equilibrium is described as what follows:

$$\frac{d}{ds} \left[ EI_3 \left( \frac{d\theta}{ds} - \frac{d\theta_0}{ds} \right) \right] + T_2 + m_3 = 0, \tag{13}$$

where  $T_2$  is now computed as function of the external load and is known.

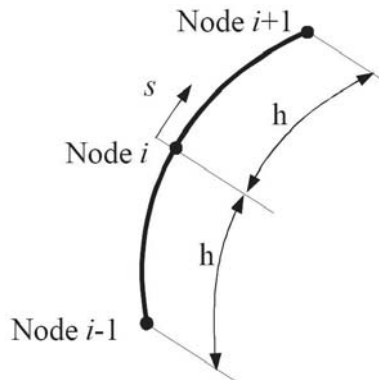


Figure 3: The special beam finite element with three nodes used to implement the non incremental formulation

A special iso-parametric beam finite element (referred to as SFET [Barraco and Munteanu (2002a,b)]) is used. It includes only one degree of freedom per node, namely the rotation  $\theta$ . The shape function  $\mathbf{N}$  of the finite element correlates the

rotation of each point of the beam,  $\theta(s)$ , to the nodal rotations of the finite element  $\theta_e$ :

$$\theta(s) = \mathbf{N}(s) \theta_e, \tag{14}$$

where (Fig.3):

$$\mathbf{N}(s) = \begin{bmatrix} \frac{s^2}{2h^2} - \frac{s}{2h} \\ -\frac{s^2}{h^2} + 1 \\ \frac{s^2}{2h^2} + \frac{s}{2h} \end{bmatrix}^T \quad \theta_e = \begin{bmatrix} \theta_{i-1} \\ \theta_i \\ \theta_{i+1} \end{bmatrix}. \tag{15}$$

Curvature  $\chi_3$  is computed by means of the above defined shape functions as:

$$\begin{aligned} \chi_3(s) &= \frac{d\theta}{ds} = \left(\frac{s}{h^2} - \frac{1}{2h}\right) \theta_{i-1} \\ &\quad - \frac{2s}{h^2} \theta_i + \left(\frac{s}{h^2} + \frac{1}{2h}\right) \theta_{i+1} \\ &= \mathbf{B} \theta_e. \end{aligned} \tag{16}$$

The finite element assembly shall include a number of  $n$  nodes, thus the first variation of the total potential energy becomes:

$$\begin{aligned} \delta\Pi &= \delta\theta_s^T \sum_{i=1}^n (EI_3 \int_l \mathbf{B}^T \mathbf{B} ds) \theta_s + \\ &\quad - \delta\theta_s^T \sum_{i=1}^n (EI_3 \int_l \mathbf{B}^T \chi_{30} ds) + \\ &\quad - \delta\theta_s^T (\mathbf{C}_e + \mathbf{C}) = 0. \end{aligned} \tag{17}$$

$\mathbf{C}_e$  is the vector of the equivalent nodal moments, which replace the distributed external forces  $\mathbf{p}$  and concentrated forces, where present. Vector  $\mathbf{C}$  contains the nodal moments replacing the distributed moments  $m_3$ . Concentrated moments will be added directly to vector  $\mathbf{C}$ . An additional term was introduced to take into account for the possibility of an initial curvature of the microbeam due to microfabrication. This contribution corresponds to the second integral written, where appears the initial curvature  $\chi_{30}$ . The nodal rotation vector, for the whole beam is  $\theta_s$ . The displacements of two sequential nodes, along the microbeam, are:

$$\begin{aligned} \mathbf{u}_{i+1} &= \mathbf{u}_i + \int_0^h \begin{bmatrix} 1 - \cos \theta \\ \sin \theta \end{bmatrix} ds \\ &\approx \mathbf{u}_i + \mathbf{H}_{i,i+1}(\theta_s). \end{aligned} \tag{18}$$

The linear displacements are  $\mathbf{u} = [u, v]^T$ . The vector  $\mathbf{H}_{i,i+1}$  is obtained as result of a numerical integration, by using the shape function of Eq. (14). Displacements can be computed by repeating several times the recursive equation (18):

$$\mathbf{u}_i = \mathbf{u}_0 + \mathbf{H}_i(\theta_s). \tag{19}$$

Subscript 0 indicates the beam end, being the origin of the curvilinear coordinate  $s$ . In present case  $u_0 = 0$ , therefore displacements and their first variation are:

$$\begin{aligned} \mathbf{u}_i &= \mathbf{H}_i(\theta_s) \\ \delta \mathbf{u}_i &= \delta \mathbf{H}_i(\theta_s) = \frac{\partial \mathbf{H}_i}{\partial \theta_s} \delta \theta_s. \end{aligned} \tag{20}$$

$\mathbf{H}_i$  is a  $2 \times 1$  array, while  $\frac{\partial \mathbf{H}_i}{\partial \theta_s}$  is a  $2 \times n$  matrix, where  $n$  is the number of nodes. The contribution of the distributed force  $\mathbf{p}(s)$ , see Eq. (11), for any virtual displacement, can be written as:

$$\begin{aligned} \int_0^l \delta \mathbf{u}^T \mathbf{p} ds &\approx \sum_{i=1}^n A_i \delta \mathbf{H}_i^T \mathbf{p}_i \\ &= \delta \theta_s^T \sum_{i=1}^n A_i \left( \frac{\partial \mathbf{H}_i}{\partial \theta_s} \right)^T \mathbf{p}_i. \end{aligned} \tag{21}$$

where  $A_i$  are known coefficients and correspond to the weights of the numerical integration. Distributed force  $\mathbf{p}$  is replaced by the equivalent nodal moment vector  $\mathbf{C}_e$  (Eq.17):

$$\mathbf{C}_e = \sum_{i=1}^n A_i \left( \frac{\partial \mathbf{H}_i}{\partial \theta_s} \right)^T \mathbf{p}_i. \tag{22}$$

Distributed moments  $m_3$  are replaced by the concentrated nodal moment  $\mathbf{C}_e$ :

$$\mathbf{C} = \sum_{i=1-h}^{n_{el}} \int^h m_3 \mathbf{N}_i^T ds. \tag{23}$$

Symbol  $\Sigma$  reminds that the standard FEM assembly procedure is applied to  $n_{el}$  elements [Barraco and Munteanu (2002a,b)].

A similar approach is used to replace the nodal concentrated forces by nodal moments. For instance, the force acting at node  $i$  is replaced by:

$$\mathbf{C}_e = \left( \frac{\partial \mathbf{H}_i}{\partial \theta_s} \right)^T \mathbf{F}_i. \tag{24}$$

Concentrated nodal moment  $C_i$ , acting at node  $i$ , is added directly to the  $i$ -th term of the loads array  $\mathbf{C}$ , defined in (23).

### 3.2 Solution Algorithm

The static analysis of the electromechanical problem of the microcantilever beam can be now performed. It is possible either solving the nonlinear equation (9) or (12), by means of the finite differences method (FDM), or by the finite element method (FEM). In the latter case, the first variation of the total potential energy is used [Barraco and Munteanu (2002a,b)]. Since the microcantilever has a free end, for each iteration, axial and shear efforts are easily evaluated, directly starting from the external load. In this case it is easy applying the Timoshenko's beam model instead of the Euler-Bernoulli's one.

Although rotation angle  $\theta$  may be large, shear angle  $\vartheta$  is usually small (Fig.2). Therefore according to Eq.(13) it follows:

$$\frac{d}{ds} \left[ EI_3 \left( \frac{d\theta}{ds} - \frac{d\theta_0}{ds} \right) \right] + (T_2 + m_3)(1 + \varepsilon_0)^2 = 0. \tag{25}$$

The first variation of total potential energy (11) is:

$$\begin{aligned} \delta\Pi = & \frac{1}{EA} \int_l \delta N N ds + \frac{1}{GA_2} \int_l \delta T_2 T_2 ds + \\ & + EI_3 \int_l \delta \Delta \chi_3 \Delta \chi_3 ds - \int_l \delta \mathbf{u}^T \mathbf{p} ds + \\ & - \int_l \delta \theta m_3 ds = 0, \end{aligned} \tag{26}$$

where actions  $N$  and  $T_2$  are known at each iteration and depend on the nodal unknowns rotations  $\theta_s$ .

Equation (18) becomes:

$$\begin{aligned} \mathbf{u}_{i+1} &= \mathbf{u}_i + \int_0^h \left( \begin{bmatrix} \cos(\theta + \vartheta) \\ \sin(\theta + \vartheta) \end{bmatrix} (1 + \varepsilon_0) - \begin{bmatrix} 1 \\ 0 \end{bmatrix} \right) ds \\ &= \mathbf{u}_i + \mathbf{H}_{i,i+1}(\theta_s), \end{aligned} \tag{27}$$

where  $\varepsilon_0 = \frac{N}{EA}$  and  $\vartheta = \frac{T_2}{GA_2}$ .

Having only one degree of freedom per node is an advantage of this approach and it applies to both Euler-Bernoulli's and Timoshenko's beam models. The computational time required to solve the coupled problem is fairly short. The discretized equilibrium equations are:

$$\mathbf{K}(\theta_s) \theta_s = \mathbf{F}, \tag{28}$$

where  $\mathbf{K}$  is the secant stiffness matrix and  $\mathbf{F}$  is the vector of the generalized forces. This method demonstrates to be very accurate. Convergence is assured and fast. Equations describing the static deformation of the beam are exact and written for the actual deformation. These features motivate to refer this approach as *non incremental*. One load step is usually sufficient to reach the final load value. To solve the nonlinear system (28), the iterative Newton-Raphson method is used, and few iterations are required to reach the convergence [De Bona and Enikov (2006)]. In case of electromechanical nonlinear coupling a sequential algorithm can be implemented in connection with the structural solution just described. Since the sequential procedure applies even to the next approach, it will be described in the following section.

#### 4 Discrete geometric approach for the coupled problem

A sketch of the 2D domain geometry is shown in Fig. 4 for the electrical-mechanical coupled problem. The domain of interest has been partitioned into the mechanical  $D_M$  and the electrical  $D_E$  domains. In  $D_M \cup D_E$ , we will introduce a pair of interlocked cell complexes based on triangles, [Bossavit and Kettunen (2000); Tonti (1988)].

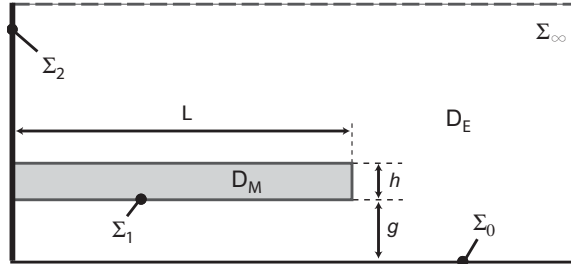


Figure 4: Sketch of the 2D electrical ( $D_E$ ) and mechanical ( $D_M$ ) domains (not on scale). The boundary  $\Sigma_1$  and  $\Sigma_0$  of the conducting domain is shown in addition.  $\Sigma_\infty$  is the truncation of the infinity domain of the electrostatic problem. Finally, on  $\Sigma_2$  the Neumann boundary condition is imposed.

Without losing generality, we focus on a triangular element  $t$ , Fig. 5. The primal complex consists of the nodes  $n_1, n_2, n_3$  of  $t$ , and of the additional nodes  $n_4, n_5, n_6$  forming the center of mass of the edges of  $t$ . The primal edges are obtained by splitting in two halves each of the edges of  $t$ . In order to assure a second order convergence in terms of electric field  $E$  and electric flux density  $D$  in  $D_E$ , or in

terms of strain  $\varepsilon_x, \varepsilon_y, \gamma$  and stress  $\sigma_x, \sigma_y, \tau$  components in  $D_M$ , we will construct a dual cell complex starting from special points in each of the edges of  $t$ , [Tonti (2002)]; these points coincide with the pair of points for the entire edge of  $t$  of a Gauss integration formula of second degree.

We denote with  $(x_i, y_i)$ , with  $i = 1, \dots, 6$  the Cartesian global coordinates of node  $n_i$ . We introduce in  $t$  a local affine reference frame  $(\xi, \eta)$  as shown in Fig. 5.

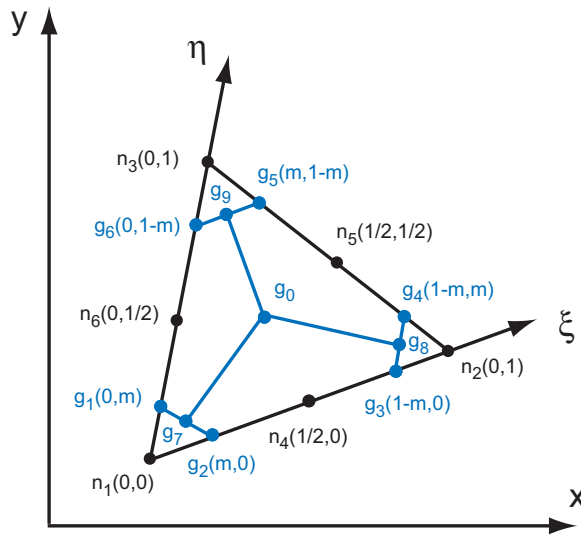


Figure 5: Global cartesian coordinate system  $(x, y)$  and local affine coordinate system  $(\xi, \eta)$  for the triangle  $t$ . Special Gauss points  $g_i, i = 1, \dots, 6$  on the edges of the triangle are shown. Finally  $g_0$  denotes the center of mass of  $t$ .

The relation between the local coordinates  $(\xi, \eta)$  of a point in  $t$  and the corresponding global coordinates  $(x, y)$ , is

$$\begin{bmatrix} x \\ y \end{bmatrix} = \begin{bmatrix} x_1 \\ y_1 \end{bmatrix} + \mathbf{T} \begin{bmatrix} \xi \\ \eta \end{bmatrix}, \tag{29}$$

where the transformation matrix  $\mathbf{T}$  is defined as

$$\mathbf{T} = \begin{bmatrix} x_2 - x_1 & x_3 - x_1 \\ y_2 - y_1 & y_3 - y_1 \end{bmatrix}. \tag{30}$$

Along each of the edges of  $t$  we denote with  $g_h, g_k$  the pair of Gauss points. For example, with reference to the edge from  $n_1$  to  $n_2$ , we write  $g_1 = (m, 0), g_2 =$

$(1 - m, 0)$ , with  $m = \frac{1}{2} - \frac{1}{2\sqrt{3}}$ . The center of mass of  $t$  is denoted with  $g_0$ . The center of mass of the edges between the pair of points  $(g_1, g_2)$ ,  $(g_3, g_4)$ ,  $(g_5, g_6)$  are denoted with  $g_7, g_8, g_9$ , respectively.

In the 2D model, a dual surface  $\tilde{s}_{hk}$  has a unitary thickness in the out of plane direction and its trace is a line segment from node  $g_h(\xi_h, \eta_h)$  to node  $g_k(\xi_k, \eta_k)$ . The components  $(\tilde{s}_x, \tilde{s}_y)$  of the area vector<sup>1</sup>  $\tilde{s}_{hk}$  of  $\tilde{s}_{hk}$  are defined as

$$\begin{bmatrix} \tilde{s}_x \\ \tilde{s}_y \end{bmatrix} = \begin{bmatrix} 0 & -1 \\ 1 & 0 \end{bmatrix} \mathbf{T} \begin{bmatrix} \xi_k - \xi_h \\ \eta_k - \eta_h \end{bmatrix}. \quad (31)$$

Next, we introduce a dual volume  $\tilde{v}_i$ , in a one to one correspondence with  $n_i$ . Its boundary is a collection of  $\tilde{s}_{hk}$  facing  $n_i$  and it is oriented by the outer normal<sup>2</sup>.

#### 4.1 Electrostatics

A synthetic tool that gives relevance to the geometrical aspects of the discrete geometric approach, and allows to derive the algebraic equations of electrostatics, is the Tonti's diagram [Tonti (1975)].

On the right side of the diagram (Fig. 6) a vertical pillar is drawn, where each DoF-array<sup>3</sup> is associated with the corresponding geometric element of the dual cell complex (from nodes  $\tilde{n}$  to volumes  $\tilde{v}$ , from bottom to top). On the left side of the diagram, a vertical pillar is drawn as well, where each DoF-array<sup>4</sup> is associated with the corresponding geometric element of the primal complex (from nodes  $n$  to volumes  $v$ , from top to bottom). The dashed circles represent categories of variables not used in this specific problem. Along a vertical pillar, we move from the variables on one level to the variables on the successive level –for example from potentials  $\mathbf{V}$  on nodes  $n$  to voltages  $\mathbf{U}$  on edges  $e$ – of the primal or of the dual complex, using the incidence matrices. This process allows us to form, at each level, algebraic *balance* relations between variables of the same category –configuration or source– yielding the physical laws in discrete form: Faraday's law  $\mathbf{C}\mathbf{U} = 0$  which is identically satisfied by introducing a potential  $\mathbf{V}$  such that  $-\mathbf{G}\mathbf{V} = \mathbf{U}$  and Gauss' law  $\tilde{\mathbf{D}}\Psi = \mathbf{Q}$ . The discrete counterpart of the constitutive relation is a square matrix  $\mathbf{M}_e$ , represented as horizontal link from left to right, which maps the array  $\mathbf{U}$  associated with primal edges  $e$  to the array  $\Psi$  associated with dual faces  $\tilde{f}$ , being in a one-to-one correspondence each other; it can be constructed in different ways as described in [Tonti (1975); Tarhasaari, Kettunen, and

<sup>1</sup> The area vector has amplitude equal to the area of  $\tilde{s}_{hk}$  and it is normal to  $\tilde{s}_{hk}$  with a specified orientation.

<sup>2</sup> For example, (refer to Fig. 5) for  $n_5$ ,  $\tilde{v}_5$  is bounded by  $\tilde{s}_{48}$ ,  $\tilde{s}_{80}$ ,  $\tilde{s}_{09}$  and  $\tilde{s}_{59}$ .

<sup>3</sup> These DoF-arrays are called *source* variables.

<sup>4</sup> These DoF-arrays are called *configuration* variables.

Bossavit (1999); Clemens, Wilke, Benderskaya, De Gersem, Koch, and Weiland (2004); Steinmetz, Helias, Wimmer, Fichte, and Clemens (2006); Bettini and Trevisan (2003); Bellina, Bettini, Tonti, and Trevisan (2002); Marrone (2007); Codicasa, Specogna, and Trevisan (2007); Clemens and Weiland (2001); Specogna and Trevisan (2005); Trevisan (2005)], under the hypothesis of element-wise uniform fields and element-wise homogeneous permittivity of the media.

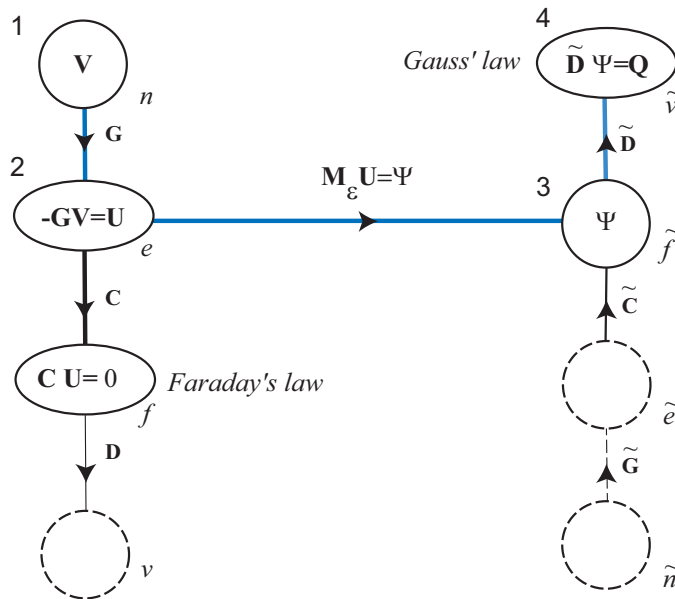


Figure 6: Tonti’s diagram for electrostatics. The incidence matrices  $\mathbf{D}$ ,  $\tilde{\mathbf{G}}$  and  $\tilde{\mathbf{C}}$  are reported for completeness, even though they are not explicitly used in this formulation.

We can now derive the set of equations governing the electrostatic problem. For each  $t \in D_E$ , the DGA for electrostatics can be cast in terms of the electric potential  $V$  (associated with a primal node  $n$ ) together with the electric flux  $\Psi$  (associated with a dual face  $\tilde{s}$ ) and the electric charge  $Q$  (associated with a dual volume  $\tilde{v}$ ). We assume here that no free charge is present in  $D_E$ , and then  $Q = 0$  for each  $\tilde{v}_i$ .

In the local coordinate system  $(\xi, \eta)$ ,  $V$  is approximated with a second order polynomial

$$V(\xi, \eta) = [1 \quad \xi \quad \eta \quad \xi^2 \quad \xi\eta \quad \eta^2] [a_1 \dots a_6]^T, \tag{32}$$

where the coefficients  $\mathbf{a} = [a_1 \dots a_6]^T$  can be computed in terms of the electric

voltages  $\mathbf{V} = [V_1 \dots V_6]^T$  at the six primal nodes of  $t$ ; in this way we obtain

$$\mathbf{a} = \mathbf{C}\mathbf{V}, \quad (33)$$

where  $\mathbf{C}$  is the resulting  $6 \times 6$  matrix. Then,  $V$  can be expressed as

$$V(\xi, \eta) = [1 \quad \xi \quad \eta \quad \xi^2 \quad \xi\eta \quad \eta^2] \mathbf{C}\mathbf{V}. \quad (34)$$

From (34), the components of  $E$  along  $(x, y)$  are

$$\begin{aligned} \begin{bmatrix} E_x \\ E_y \end{bmatrix} &= - \begin{bmatrix} \partial_x V \\ \partial_y V \end{bmatrix} = -\mathbf{J} \begin{bmatrix} \partial_\xi V \\ \partial_\eta V \end{bmatrix} \\ &= -(\mathbf{T}^{-1})^T \mathbf{N}\mathbf{C}\mathbf{V}, \end{aligned} \quad (35)$$

where  $\mathbf{J}$  is the Jacobian matrix of the mapping from  $(\xi, \eta)$  to  $(x, y)$  coordinates, and the matrix  $\mathbf{N}$  is defined as

$$\mathbf{N} = \begin{bmatrix} 0 & 1 & 0 & 2\xi & \eta & 0 \\ 0 & 0 & 1 & 0 & \xi & 2\eta \end{bmatrix}. \quad (36)$$

Denoting with  $\Psi_{hk} = \int_{\tilde{s}_{hk}} \mathbf{D} \cdot d\mathbf{s}$  the electric flux of  $\mathbf{D}$  through  $\tilde{s}_{hk}$ , we get

$$\Psi_{hk} = \begin{bmatrix} \tilde{s}_x & \tilde{s}_y \end{bmatrix} \begin{bmatrix} D_x \\ D_y \end{bmatrix}, \quad (37)$$

where  $D_x$  and  $D_y$  are the components of  $\mathbf{D}$  evaluated in the center of mass of  $\tilde{s}_{hk}$ . By substituting in (37), (31) for the components of  $\tilde{s}_{hk}$ , using the constitutive relation  $\mathbf{D} = \varepsilon\mathbf{E}$ , with  $\varepsilon$  the uniform permittivity of  $t$ , and evaluating the components of  $\mathbf{E}$  according to (35), we obtain

$$\Psi_{hk} = -\tilde{s}_{hk}\varepsilon(\mathbf{T}^{-1})^T \mathbf{N}\mathbf{C}\mathbf{V}, \quad (38)$$

where  $\varepsilon$  is a constant for homogeneous, isotropic and linear dielectric material inside each primal cell, or it is a tensor in the general case.

Next, for element  $t$  we may write the local contribution to Gauss' Law as

$$\tilde{\mathbf{D}}\Psi = 0, \quad (39)$$

where  $\tilde{\mathbf{D}}$  is the matrix of incidence numbers between the outer orientation of  $\tilde{v}_i$  and the outer orientation of  $\tilde{s}_{hk}$ .

Finally, assembling the contribution from (39) for each  $t$ , the final system becomes

$$\mathbf{K}_E \mathbf{V} = 0, \quad (40)$$

where  $\mathbf{K}_E$  is the resulting stiffness matrix for the electrostatic problem. The boundary conditions must be assigned to close the problem in  $D_E$ , by prescribing  $V_1 = V$  for the potential on  $\Sigma_1$ ,  $V_0 = 0$  for the potential on  $\Sigma_0 \cup \Sigma_\infty$ , and zero electric flux on  $\Sigma_2$ .

From the solution of (40), the components of the electrostatic force acting on  $n_i$  laying on  $\Sigma_1$  can be evaluated as

$$\begin{bmatrix} F_x \\ F_y \end{bmatrix} = \frac{1}{2} Q_i \begin{bmatrix} E_{ax} \\ E_{ay} \end{bmatrix}, \tag{41}$$

where  $Q_i$  is the surface charge lying on the conducting boundary  $\Sigma_1$  in the neighborhood of node  $n_i$  and  $E_{ax}, E_{ay}$  are the components of the average electrical field acting on  $n_i$ .

#### 4.2 Elastostatics

For each  $t \in D_M$ , the DGA for elastostatics can be cast in terms of the components  $U_x$  and  $U_y$  of the displacement vector (associated with a primal node  $n$ ), together with the surface force vector  $F$  (associated with a dual face  $\bar{s}$ ). Again, we approximate  $U_x, U_y$  as

$$[U_x \ U_y] = [1 \ \xi \ \eta \ \xi^2 \ \xi\eta \ \eta^2] \mathbf{C} [U_x \ U_y], \tag{42}$$

where  $\mathbf{U}_x, \mathbf{U}_y$  are the arrays of the displacement components in the primal nodes. From (42), the displacement gradient components along the axes of the global coordinate system  $(x, y)$  are

$$[H_x \ H_y] = \begin{bmatrix} \partial_x U_x & \partial_x U_y \\ \partial_y U_x & \partial_y U_y \end{bmatrix} = \begin{bmatrix} \mathbf{B}_1 \\ \mathbf{B}_2 \end{bmatrix} [U_x \ U_y], \tag{43}$$

where

$$\begin{bmatrix} \mathbf{B}_1 \\ \mathbf{B}_2 \end{bmatrix} = (\mathbf{T}^{-1})^T \mathbf{N} \mathbf{C}. \tag{44}$$

Then, the strain components can be written as

$$\begin{bmatrix} \varepsilon_x \\ \varepsilon_y \\ \gamma \end{bmatrix} = \begin{bmatrix} \mathbf{B}_1 & 0 \\ 0 & \mathbf{B}_2 \\ \mathbf{B}_1 & \mathbf{B}_2 \end{bmatrix} \begin{bmatrix} U_x \\ U_y \end{bmatrix} = \mathbf{B} \begin{bmatrix} U_x \\ U_y \end{bmatrix}, \tag{45}$$

where the symmetric part of the displacement gradient matrix is obtained thanks to the structure of  $\mathbf{B}$ .

Using Hook's Law between stress and strain components and (45), we obtain

$$\begin{bmatrix} \sigma_x \\ \sigma_y \\ \tau \end{bmatrix} = \mathbf{P} \begin{bmatrix} \varepsilon_x \\ \varepsilon_y \\ \gamma \end{bmatrix} = \mathbf{P} \mathbf{B} \begin{bmatrix} \mathbf{U}_x \\ \mathbf{U}_y \end{bmatrix} \quad (46)$$

where  $\sigma_x$ ,  $\sigma_y$ ,  $\tau$  are the stress components acting on  $\tilde{s}_{hk}$  and  $\mathbf{P}$ , in the case of 2D plain stress, for isotropic homogeneous material, is given by

$$\mathbf{P} = \frac{E}{(1+\nu)(1-2\nu)} \begin{bmatrix} 1-\nu & \nu & 0 \\ \nu & 1-\nu & 0 \\ 0 & 0 & \frac{1-2\nu}{2} \end{bmatrix}. \quad (47)$$

Next, the surface force array  $\mathbf{F}_{hk} = [F_x \ F_y]^T$  on  $\tilde{s}_{hk}$  is

$$\mathbf{F}_{hk} = \begin{bmatrix} \tilde{s}_x & 0 & \tilde{s}_y \\ 0 & \tilde{s}_y & \tilde{s}_x \end{bmatrix} \begin{bmatrix} \sigma_x \\ \sigma_y \\ \tau \end{bmatrix} = \tilde{\mathbf{S}} \begin{bmatrix} \sigma_x \\ \sigma_y \\ \tau \end{bmatrix}, \quad (48)$$

where  $\sigma_x$ ,  $\sigma_y$  and  $\tau$  are evaluated in the center of mass of  $\tilde{s}_{hk}$ . Then, for element  $t$  we may write the local equilibrium equations, in the absence of volume forces, yielding

$$\tilde{\mathbf{D}} [ \mathbf{F}_x \ \mathbf{F}_y ] = 0, \quad (49)$$

where  $\mathbf{F}_x$ ,  $\mathbf{F}_y$  are respectively the array of the  $F_x$ ,  $F_y$  components of the resulting surface force. Each balance equation (49) is associated with dual volumes and is in a one-to-one correspondence with a primal node  $n_i$ .

Finally, assembling the contribution from (49) for each  $t$ , the final system becomes

$$\mathbf{K}_M \mathbf{U} = \mathbf{F}, \quad (50)$$

where  $\mathbf{U} = [ \mathbf{U}_x^T \ \mathbf{U}_y^T ]^T$ , and  $\mathbf{F}$  is the array of the mechanical loads with non null entries on the nodes  $n_i \in \Sigma_1$  only, calculated according to (41);  $\mathbf{K}_M$  is the resulting stiffness matrix for the elastostatic problem. In addition, the constraints  $U_x = 0$ ,  $U_y = 0$  are imposed for  $n_i \in D_M \cap \Sigma_2$ .

The Tonti's diagram [Tonti (1975)] for elastostatics is shown in Fig. 7; the dashed circles represent categories of variables not used in this specific problem.

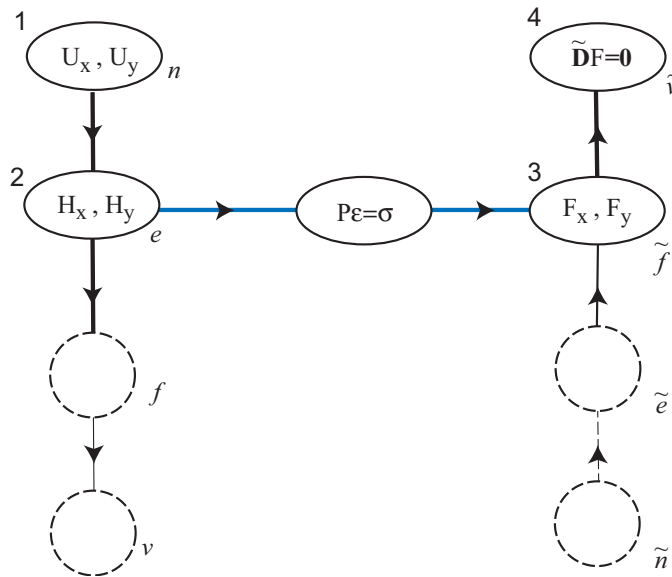


Figure 7: Tonti's diagram for elastostatics.

### 4.3 Solution Algorithm

An efficient, fast and robust relaxation algorithm has been developed to analyze the electromechanical non linear problem presented hereafter. The two domains  $D_M$  and  $D_E$  mutually influence each other only at the interface, so that an iterative sequential analysis of the two fields can be suitably performed. A sequential field coupling (SFC) approach with voltage increments is adopted (see Fig. 8). The total potential difference is split into  $n$  increments: for each intermediate voltage value  $V_i$  the coupled analysis is performed by means of the usual SFC method. The applied potential difference is increased only after equilibrium configuration is achieved.

## 5 Numerical results and comparisons

To evaluate the actual effectiveness of the new proposed approaches, a comparison has been performed among several nonlinear solutions. They were obtained by means of the non incremental algorithm, based on the special beam element SFET, by the discrete geometric approach DGA and by a commercial FEM code (ANSYS). The tested problem is fully 3D, mainly because of the distribution of the electrostatic loads on the microbeam. Nevertheless, the comparison is based on 2D analyses to investigate their effectiveness with respect to the complete 3D models. The aim is to investigate the possibility of building a fast and reliable 2D model

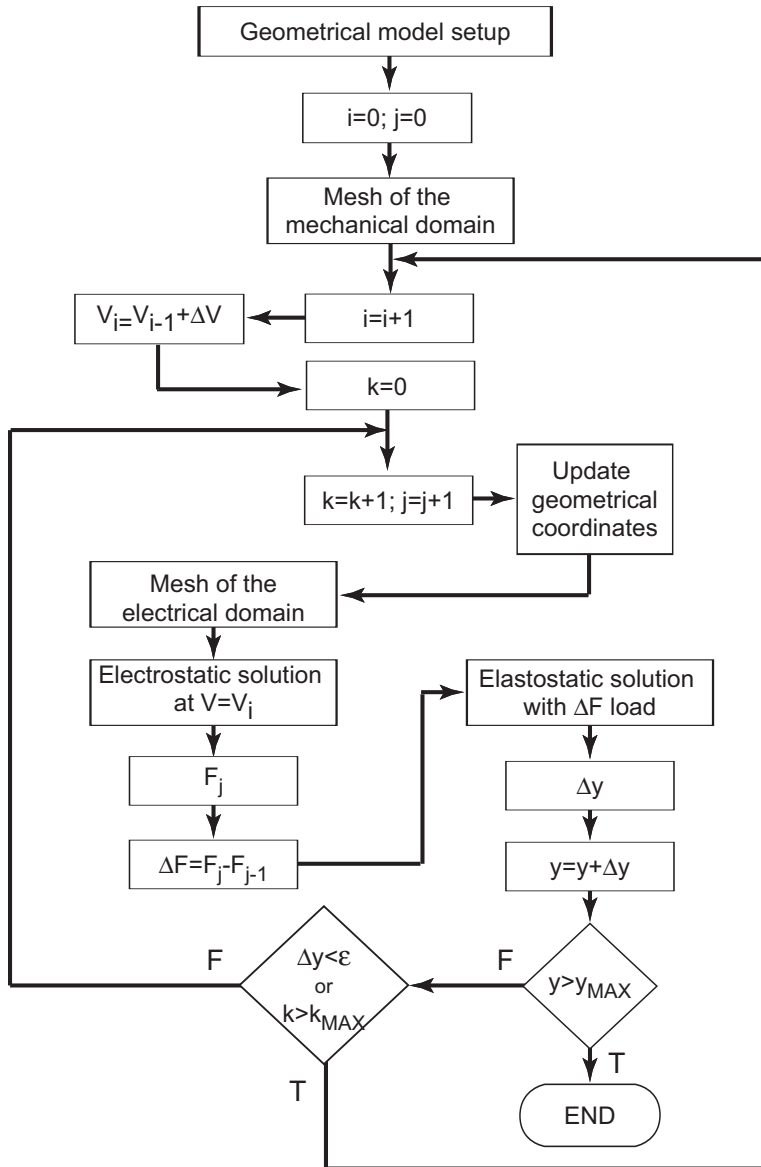


Figure 8: Flowchart of the sequential field coupling DGA approach implemented with voltage increments. The internal loop (indexed with  $k$ ) describes the increments of loads  $\Delta F$ , while the outer loop (indexed with  $i$ ) describes the increments  $\Delta V$  applied to the voltage.

suitable to approximate, with enough accuracy, the actual 3D behaviour of several specimens experimentally tested. A challenging aspect of the proposed approach is the development of a compact model, useful to predict the dynamic behaviour of the electromechanical coupled microsystem, where both electromechanical and geometrical nonlinearities are present simultaneously.

Practical cases used to perform the experimental validation are Epitaxial Polysilicon cantilever microbeams (Young modulus  $E = 150 \div 166 \text{ GPa}$ , Poisson coefficient  $\nu=0.23$ ). Several cases have been considered as shown in table 1 for different values of microbeam length ( $L$ ), gap ( $g$ ), thickness ( $h$ ) and depth ( $d$ ).

As far as Table 1 shows the accuracy of the profiling system in case of in-plane bending test allows characterizing the dimensions of the microbeam actuators with a very good resolution along the optical axis, while it is far less on the target plane. Therefore all the dimensions measured in the target plane suffer a certain inaccuracy in measuring, which was resumed in Table 1 [Ballestra, Brusa, Munteanu, and Somà (2008); Brusa, Della Gaspera, and Munteanu (2008)].

Table 1: Polysilicon cantilever microbeams. Different values of length ( $L$ ), gap ( $g$ ), thickness ( $h$ ), depth ( $d$ ) have been considered.

case	$L [\mu m]$	$g [\mu m]$	$h [\mu m]$	$d [\mu m]$
1	$101 \pm 0.1$	$5.0 \pm 0.3$	$1.8 \pm 0.02$	15
2	$101 \pm 0.1$	$10.0 \pm 0.3$	$1.8 \pm 0.02$	15
3	$101 \pm 0.1$	$20.1 \pm 0.3$	$1.8 \pm 0.02$	15
4	$205 \pm 0.2$	$10.0 \pm 0.3$	$1.9 \pm 0.02$	15
5	$205 \pm 0.2$	$20.0 \pm 0.3$	$1.9 \pm 0.02$	15
6	$805 \pm 0.5$	$39.6 \pm 0.3$	$2.7 \pm 0.04$	15
7	$805 \pm 0.5$	$200.0 \pm 0.5$	$2.7 \pm 0.04$	15
8	$805 \pm 0.5$	$400.0 \pm 0.5$	$2.7 \pm 0.04$	15

It is important to notice that the behaviour is geometrically nonlinear, thus requiring to implement the iterative solution to solve the nonlinear mechanical problem, corresponding to the large displacement condition. This leads to the maximum computational time, when static solution to compute the pull-in is performed.

### **5.1 Validation**

Figure 9, 10, 11 compare the experimental tip displacement, as a function of the applied voltage, with numerical predictions for test cases 2, 4, and 6 of table 1 respectively. A quite good agreement is shown among the numerical results calculated by non incremental FEM model, by DGA and by a commercial FEM code (ANSYS) for given values of the Young modulus ( $E$ ). The experimental measures lie between the curves calculated with the lower ( $E=150\text{ GPa}$ ) and upper ( $E=166\text{ GPa}$ ) bounds assumed for Epitaxial Polysilicon cantilever microbeams. The pull-in voltage and displacement are both quite accurately predicted.

The non incremental approach, which was initially developed in MATLAB environment, takes approximately 1/3 the time spent by a sequential solution, implementing the classic beam element, to compute the displacement at pull-in. The nonlinear dynamic response in presence of large vibration is only possible by means of this non incremental approach, since the double nonlinear model (geometrical and electromechanical) in dynamic domain cannot be solved by the currently available commercial codes [Munteanu and Brusa (2005)]. Although a complete validation in dynamic behavior prediction will be possible only when both commercial sequential approach and DGA will add the suitable subroutines, the computational time, the required mesh refinement and the numerical convergence of both non incremental and DGA methods look to be promising. Other direct comparisons of the performance in terms of efficiency and computational time with the other methods are currently unpractical since models have been developed in different environments (ANSYS, Matlab, Fortran).

## **6 Conclusions**

This paper deals with the application of the FE sequential and non-incremental method and of the Discrete Geometric Approach to the numerical prediction of the nonlinear behaviour of electrostatic microactuators. Planar static solution demonstrates that the performance of DGA is very competitive and assures the same level of accuracy of available methods like FEM coupled-field solution, sequential non incremental FEM and FEM-BEM hybrid method. Sequential non incremental FEM modelling is faster than the commonly used sequential approach implemented in commercial codes. Up to now a dynamic analysis in presence of large displacement and geometrical nonlinearity looks only possible by means of this approach. At present, the validation has been mainly based on the static solution, because of the larger information available from the different methods. Numerical results agree very well, even with the experimental ones. Validation was used to define the limits of application of the 2D models. These are mainly due to the actual

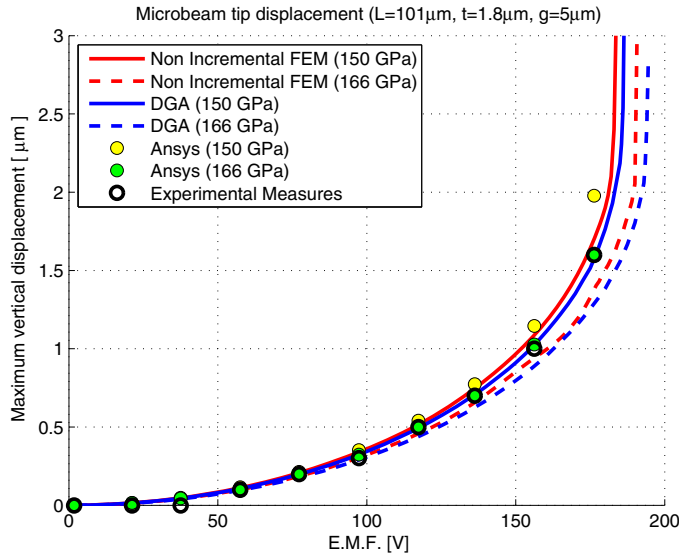


Figure 9: Comparison of experimental tip displacement with numerical predictions. Test case 2:  $L = 101\mu\text{m}$ ,  $h = 1.8\mu\text{m}$ ,  $d = 15\mu\text{m}$ ,  $g = 10\mu\text{m}$ .

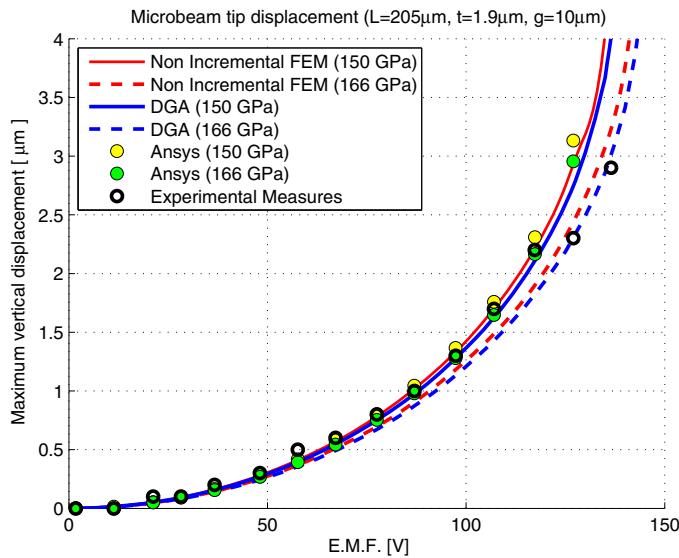


Figure 10: Comparison of experimental tip displacement with numerical predictions. Test case 4:  $L = 205\mu\text{m}$ ,  $h = 1.9\mu\text{m}$ ,  $d = 15\mu\text{m}$ ,  $g = 10\mu\text{m}$ .

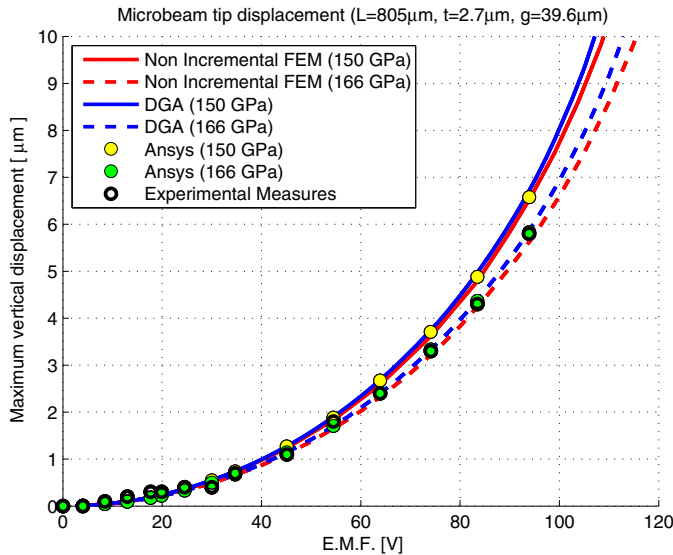


Figure 11: Comparison of experimental tip displacement with numerical predictions. Test case 6:  $L = 805\mu m$ ,  $h = 2.7\mu m$ ,  $d = 15\mu m$ ,  $g = 39.6\mu m$ ).

distribution of the electrostatic forces, affected by fringing of the electric field. It appeared remarkable that experimental results are fitted by the 2D models, if an effective value of the microbeam thickness is calibrated on the actual response, thus making 2D methods suitable candidates for a compact modelling operation of the microelectrostatic actuators.

**Acknowledgement:** This work was partially funded by the Italian Ministry of University under grant 2005/2005091729 to the Operative Unit of Udine coordinated by prof. Eugenio Brusa.

**References**

**Abdel-Raman, E. M.; Younis, M. I.; Nayfeh, A. H. (2003):** On simple formulations of weakly-singular traction & displacement bie, and their solutions through petrov-galerkin approaches. *Journal of Micromechanics and Microengineering*, vol. 12, no. 1, pp. 759–766.

**Adey, R. A.; Lahrman, A.; Le mölmann, C. (1995):** *Simulation and design of Microsystems and microstructures*. Computational Mechanics Publications, Southampton, UK.

**Ballestra, A.; Brusa, E.; Munteanu, M. G.; Somà, A.** (2008): Experimental characterization of electrostatically actuated inplane bending of microcantilevers. *J.Microsystem Technology*, vol. 14, no. 7, pp. 909–918.

**Barraco, A.; Munteanu, M. G.** (2002): A special finite element for static and dynamic study of mechanical systems under large motion, part i. *Revue Européenne des Elements Finis*, vol. 11, no. 6, pp. 773–790.

**Barraco, A.; Munteanu, M. G.** (2002): A special finite element for static and dynamic study of mechanical systems under large motion, part ii. *Revue Européenne des Elements Finis*, vol. 11, no. 6, pp. 791–814.

**Bellina, F.; Bettini, P.; Tonti, E.; Trevisan, F.** (2002): Finite formulation for the solution of a 2d eddy-current problem. *IEEE Trans. Mag.*, vol. 38, no. 2, pp. 561–564.

**Bettini, P.; Brusa, E.; Munteanu, M.; Specogna, R.; Trevisan, F.** (2008): Static behaviour prediction of microelectrostatic actuators by discrete geometric approaches. *IEEE Transactions on Magnetics*, vol. 44, pp. 1606–1609.

**Bettini, P.; Trevisan, F.** (2003): Electrostatic analysis for plane problems with finite formulation. *IEEE Trans. Mag.*, vol. 39, no. 3, pp. 1127–1130.

**Bossavit, A.** (1998): How weak is the weak solution in finite elements methods? *IEEE Trans. Mag.*, vol. 34, pp. 2429–2432.

**Bossavit, A.; Kettunen, L.** (2000): Yee-like schemes on staggered cellular grids: A synthesis between fit and fem approaches. *IEEE Trans. Mag.*, vol. 36, pp. 861–867.

**Brusa, E.; Della Gaspera, A.; Munteanu, M. G.** (2008): Validation of compact models of microcantilever actuators for rf-mems application. *Proc. IEEE,DTIP 2008; CAD, Design and Test Conference*.

**Clemens, M.; Weiland, T.** (2001): Discrete electromagnetism with the finite integration technique. *PIER 32*, pp. 65–87.

**Clemens, M.; Wilke, M.; Benderskaya, G.; De Gersem, H.; Koch, W.; Weiland, T.** (2004): Transient electro-quasistatic adaptive simulation schemes. *IEEE Trans. Mag.*, vol. 40, no. 2, pp. 1294–1297.

**Codecasa, L.; Specogna, R.; Trevisan, F.** (2007): Symmetric positive-definite constitutive matrices for discrete eddy-current problems. *IEEE Trans. Mag.*, vol. 42, no. 2, pp. 510–515.

**Cosmi, F.** (2001): Numerical solution of plane elasticity problems with the cell method. *CMES: Computer Modeling in Engineering & Sciences*, vol. 2, no. 3, pp. 365–372.

**Cui, X. Y.; Liu, G. R.; Li, G. Y.; Zhao, X.; Nguyen, T. T.; Sun, G. Y.** (2008): A smoothed finite element method (sfem) for linear and geometrically nonlinear analysis of plates and shells. *CMES: Computer Modeling in Engineering & Sciences*, vol. 28, no. 2, pp. 109–125.

**De Bona, F.; Enikov, E.** (2006): *Microsystems Mechanical Design*. Springer Verlag, Wien and New York.

**Gyimesi, M.; Ostergaard, D.** (1999): Electro-mechanical transducers for mems analysis in ansys. *MSM Conference*, pp. 270–273.

**Heshmatzadeh, M.; Bridges, G. E.** (2007): A geometrical comparison between cell method and finite element method in electrostatics. *CMES: Computer Modeling in Engineering & Sciences*, vol. 18, no. 1, pp. 45–58.

**Lee, S. Y.; Lin, S. M.; Lee, C. S.; Lu, S. Y.; Liu, Y. T.** (2008): Exact large deflection of beams with nonlinear boundary conditions. *CMES: Computer Modeling in Engineering & Sciences*, vol. 30, no. 1, pp. 27–36.

**Marrone, M.** (2007): A new consistent way to build symmetric constitutive matrices on general 2d grids. *IEEE Trans. Mag.*, vol. 40, no. 2, pp. 1420–1423.

**Munteanu, M. G.; Brusa, E.** (2005): A new fem approach to the coupled-field analysis of electrostatic microactuators dynamics. *ECCOMAS Thematic Conference on Coupled Problems, Santorini, Greece*.

**Munteanu, M. G.; De Bona, F.; Collenz, A.; Brusa, E.** (2004): Geometrical nonlinearities of electrostatically actuated microbeams. *ECCOMAS Conference, Jyväskylä, Finland*.

**Rebeiz, G.** (2003): *RF MEMS, Theory, design and technology*. Wiley Interscience, New York.

**Senturia, S. D.** (2001): *Microsystems design*. Kluwer, Boston.

**Somà, A.; Collenz, A.; De Bona, F.; Gugliotta, A.** (2004): Large deflections of microbeams under electrostatic loads. *Journal of Micromechanics and Microengineering*, vol. 14, pp. 365–373.

**Specogna, R.; Trevisan, F.** (2005): Discrete constitutive equations in  $a - \chi$  geometric eddy-currents formulation. *IEEE Trans. Magn.*, vol. 41, no. 4, pp. 1259–1263.

**Springhetti, R.; Novati, G.; Margonari, M.** (2006): Weak coupling of the symmetric galerkin bem with fem for potential and elastostatic problems. *CMES: Computer Modeling in Engineering & Sciences*, vol. 13, no. 1, pp. 67–80.

**Steinmetz, T.; Helias, M.; Wimmer, G.; Fichte, L. O.; Clemens, M.** (2006): Electro-quasistatic field simulations based on a discrete electromagnetism formulation. *IEEE Trans. Mag.*, vol. 42, no. 4, pp. 755–758.

**Tarhasaari, T.; Kettunen, L.; Bossavit, A.** (1999): Some realizations of a discrete hodge operator: A reinterpretation of finite elements techniques. *IEEE Trans. Mag.*, vol. 55, no. 3, pp. 1494–1497.

**Timoshenko, S.** (1968): *Theory of elasticity*. McGraw Hill, New York.

**Tonti, E.** (1975): *On the formal structure of physical theories*. Quaderni dei Gruppi di Ricerca Matematica del CNR.

**Tonti, E.** (1988): Algebraic topology and computational electromagnetism. *IMF Conference*, pp. 284–294.

**Tonti, E.** (2001): A direct discrete formulation of field laws: The cell method. *CMES: Computer Modeling in Engineering & Sciences*, vol. 2, no. 2, pp. 237–258.

**Tonti, E.** (2002): Finite formulation of electromagnetic field. *IEEE Trans. Mag.*, vol. 38, pp. 333–336.

**Trevisan, F.** (2005): 3-d eddy current analysis with the cell method for nde problemsn. *IEEE Trans. Magn.*, vol. 40, no. 2, pp. 1314–1317.

**Wen, P. H.; Hon, Y. C.** (2007): Geometrically nonlinear analysis of reissner-mindlin plate by meshless computation. *CMES: Computer Modeling in Engineering & Sciences*, vol. 21, no. 3, pp. 177–191.